Export Cable Protection for Offshore Wind Farms Using Type-IV Wind Turbine Generators

Ardavan Mohammadhassani[12], Nicholas Skoff[1], Tin Nguyen, P.E.[1], and Ali Mehrizi-Sani[2]
[1]Dominion Energy, [2]Virginia Tech
{ardavanmh93,mehrizi}@vt.edu and {nicholas.m.skoff,tin.nguyen}@dominionenergy.com

***Abstract*—Export cable protection for offshore wind farms (OWF) using Type-IV wind turbine generators (WTGs) is challenging due to the WTG's limited, variable, and unconventional fault-current response. Typically, line-current-differential relaying is used for primary protection and then, when communication is lost, the differential relays are backed up by distance relays. However, in presence of WTGs, distance protection is highly prone to misoperation. Therefore, this paper proposes a protection scheme that uses a loss-of-potential overcurrent logic for OWF export cables as an alternative backup protection. For this study, an experimental setup was created using a real-time digital simulator and physical relays to evaluate the performance of the proposed protection scheme using hardware-in-the-loop testing. Test results showed that the proposed scheme operated correctly under different types of faults and fault locations.**

***Index Terms*—DC-AC power converters, differential protection, distance protection, overcurrent protection, power system protection, wind energy integration.**

I. Introduction

Integration of Type-IV wind turbine generators (WTGs) in an offshore wind farm (OWF) is part of the solution for large-scale, clean and renewable production of electricity [1]. The safe and reliable delivery of power from an OWF requires that OWF export cables be protected from short-circuit faults. However, this is very challenging, as WTGs respond differently to faults than synchronous generators (SGs) do [2]-[7]. While SGs can provide a fault current as high as 3-6 pu, the maximum current output of a WTG cannot exceed 1.1-1.2 pu. A WTG also exhibits a distorted output current under unbalanced faults. Since wind is an intermittent source of energy, its fault-current contribution varies with different wind speeds. Given that conventional protection devices are designed to operate in an SG-dominated power system, they may not operate correctly in the presence of WTGs. Therefore, new protection schemes need to be designed for OWF export cables.

Various methods have been proposed to address the problem of transmission system protection in WTGs. [8] proposed an apparent impedance calculation method to find and correct the Zone 2 settings of mis-coordinated distance relays in OWFs with high-voltage, direct-current (HVDC) connections. [9] designed a robust reactive power controller for HVDC systems to avoid the misoperation of distance relays under faults in their backup zones. [10] addressed the problem of variable fault current contribution from WTGs' distance protection scheme by using a dynamic impedance plane. [11] proposed an improved distance protection method based on time delay and zero-sequence impedance. [12] proposed two new logic designs to increase the security of directional elements under balanced faults as well as the reliability of Zone 2 elements in distance relays. [13] designed a negative-sequence current response for renewable energy power plants to ensure that directional relays perform correctly under faults. [14] designed a control loop to generate a reference waveform that can be used by distance relays as polarizing voltage to ensure correct performance.-[15] suggested a dual-time, transform-assisted, intelligent relaying approach to address the protection of STATCOM-equipped transmission lines that interconnect wind farms.

Although the published literature addresses different individual issues with system protection in the presence of WTGs, none of them propose a complete export cable protection system for OWFs. Moreover, some of the proposed methods require access to the internal WTG control system, which may not always be available. Other methods may also increase the operating time of the protective relays. This paper proposes a sensitive and selective protection system for OWF export cables, where primary protection is provided by using line current differential relaying and backup protection by using distance relaying. Given that distance protection is highly vulnerable to misoperation in presence of WTGs, a loss-of-potential-based overcurrent logic is proposed in this paper as an alternative for backup protection using distance relaying. An experimental setup is created using RTDS real-time simulator and physical relays to evaluate the performance of the proposed protection system using hardware-in-the-loop (HIL) testing.

The rest of this paper is structured as follows. Section II provides an overview of WTG modeling and control as well as the employed test system. The proposed protection scheme is presented in Section III. Performance evaluation is provided in Section IV. Conclusions are provided in Section V. Finally, future work is discussed in Section VI.

II. Overview of the System Model

A. Overview of WTG Modeling and Control

This section presents the methodology used to model the WTGs. The mechanical power of the wind was converted into electrical power using a direct-driven permanent magnet synchronous generator (PMSG), which was connected to the machine side converter (MSC) using a series inductor L_m.

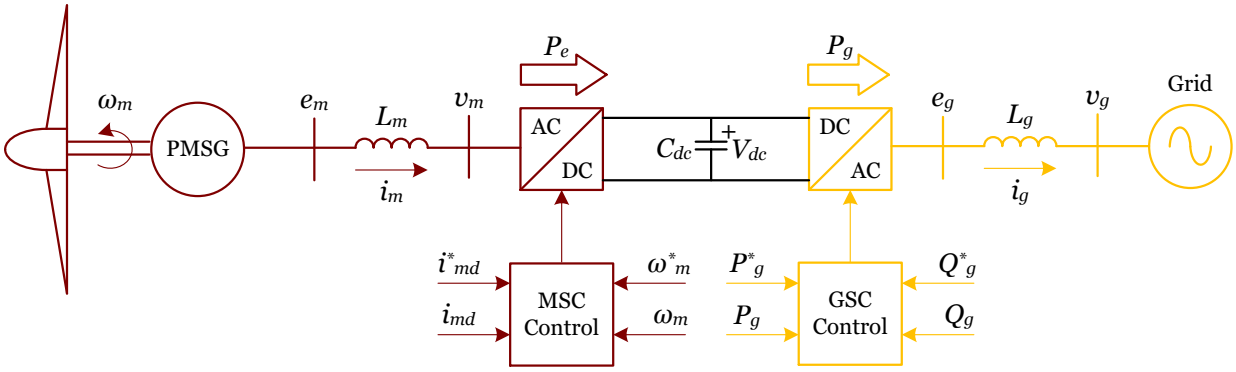

Fig. 1. Overview of the WTG model and controls.

The MSC controlled the frequency and magnitude of the machine-side voltage v_m, so that power from the PMSG P_e flowed fully into the DC-link capacitor. The mathematical model of the MSC was found in the synchronous dq frame using (1) and (2) as

$$v_{md} = e_{md} - R_m i_{md} - L_{md}\frac{di_{md}}{dt} + \omega_e L_{mq} i_{mq}, \quad (1)$$

and

$$v_{mq} = e_{mq} - R_m i_{mq} - L_{mq}\frac{di_{mq}}{dt} + \omega_e L_{md} i_{md}, \quad (2)$$

where R_m was the winding resistance and ω_e was the electrical frequency of e_m. Figs. 2(a) and (b) show the control loops for i_{md} and i_{mq}.

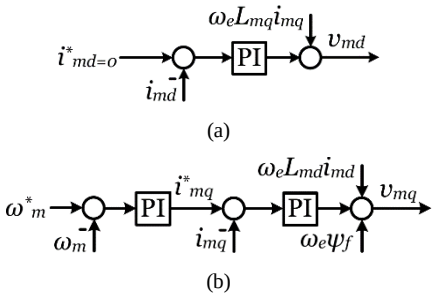

Fig. 2. MSC control system for (a) i_{md} and (b) i_{mq}.

Zero-direct-axis current control (ZDC) was used to maintain i_{md} at its set point $i^*_{md} = 0$. The control loop for i_{mq} maintained the mechanical speed of the PMSG ω_m at its set point ω^*_m by adjusting the PMSG's electromagnetic torque τ_{em} until it was equal to the mechanical torque of the turbine τ_{mec}. τ_{em} was found using (3) as

$$\tau_{em} = \frac{3}{2} p i_{mq} \psi_f, \quad (3)$$

where p was the number of PMSG pole pairs and ψ_f was the permanent magnet flux. The dynamics of the mechanical speed of the PMSG ω_m was found using (4) as

$$\tau_{mec} - \tau_{em} = J\frac{d\omega_m}{dt} = J\frac{d(p\omega_e)}{dt}, \quad (4)$$

where J was the PMSG moment of inertia. The grid-side converter (GSC) controlled the DC-link voltage so that the power injected into the grid P_g was equal to P_e. The dynamics of V_{dc} were found using (5) as

$$C_{dc}\frac{dV_{dc}}{dt} = \frac{P_e - P_g}{V_{dc}}, \quad (5)$$

where C_{dc} was the DC-link capacitance. The GSC could also provide voltage support by injecting reactive power Q_g into the grid by controlling the magnitude and frequency of the voltage e_g. The mathematical model of the GSC was found in the synchronous dq frame using (6) and (7) as

$$e_{gd} = R_g i_{gd} + L_g\frac{di_{gd}}{dt} - \omega_g L_g i_{gq} + v_{gd}, \quad (6)$$

$$e_{gq} = R_g i_{gq} + L_g\frac{di_{gq}}{dt} - \omega_g L_g i_{gd} + v_{gq}, \quad (7)$$

where R_g was the winding resistance of L_g and ω_g was the electrical frequency of the grid voltage v_g. Figs. 3(a) and (b) show the control loops for i_{gd} and i_{gq}. P_g injected to the grid was controlled at its set point P^*_g via i_{gd}, while Q_g was controlled at its set point Q^*_g via i_{gq}.

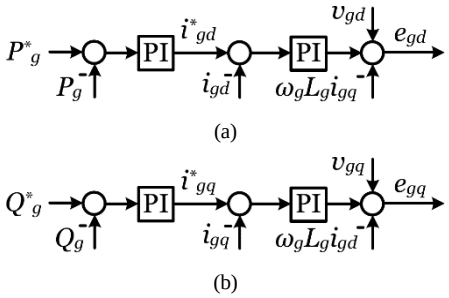

Fig. 3. GSC control system for (a) i_{gd} and (b) i_{gq}.

B. Overview of the Test System

In this section the modeling of the remaining equipment in the test system is explained. Fig. 4 shows the test system, comprising 176 WTGs, each rated at 16.7 MVA, leading to a total rating of 2.94 GVA. Three offshore substations (OSS) interconnections had three aggregated strings of approximately 20 WTGs each. Each aggregated WTG was connected to an aggregated, three-phase, submarine inter-array cable (IAC) using an aggregated 0.69 kV : 66 kV Y–Δ three-phase inverter step-up transformer (ISU).

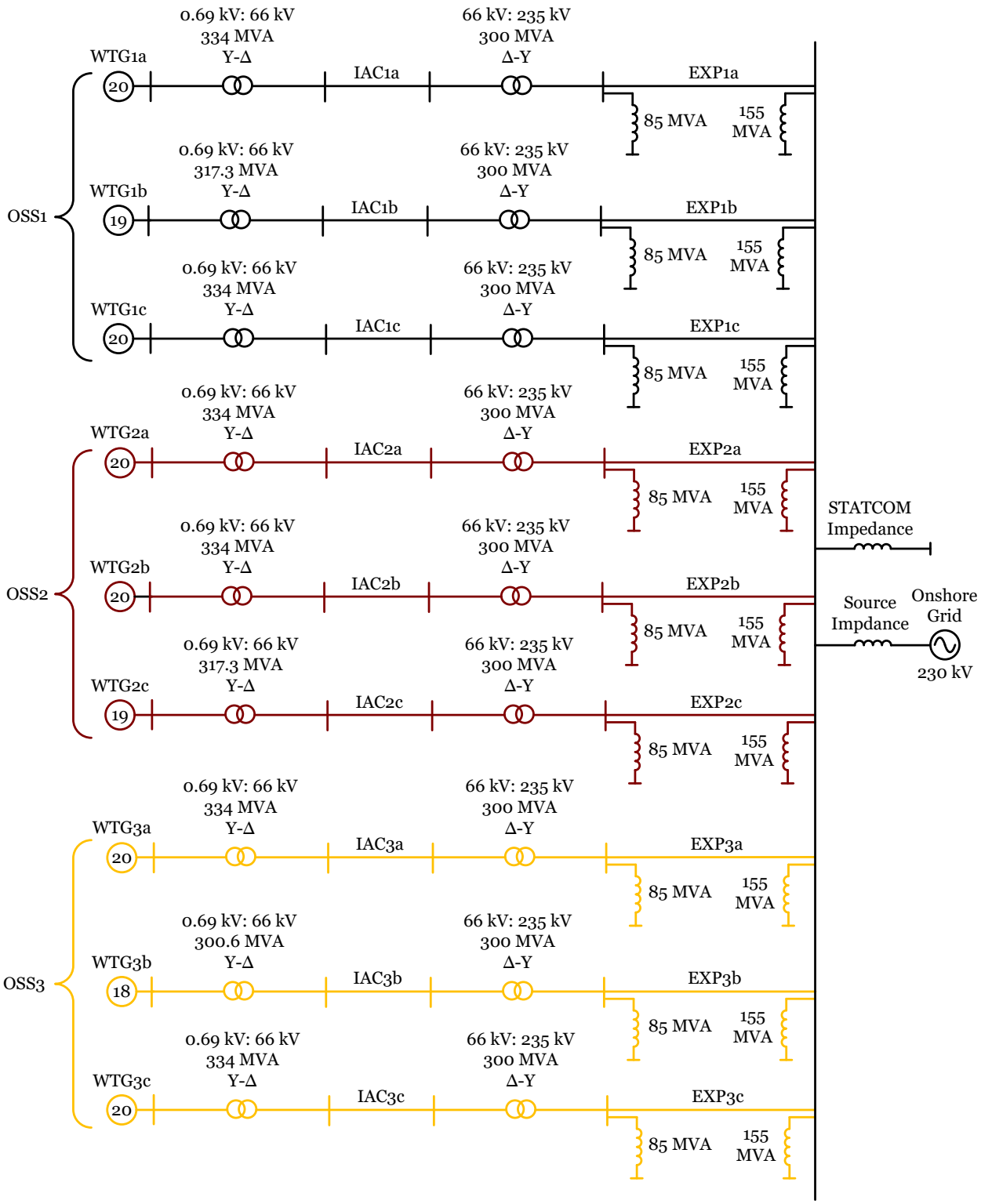

Fig. 4. Developed test system.

Although a single ISU was rated at 16.7 MVA, the rating of an aggregated ISU depended on the number of WTGs aggregated. Each aggregated IAC was then connected to a submarine export cable (EXP) via a 300 MVA 66 kV: 235 kV Δ–Y generator step-up (GSU) transformer. An 85 MVA shunt reactor was installed offshore as well as another three-phase 155 MVA shunt reactor onshore to compensate for the IAC and EXP charging currents. Three additional 250 MVA

STATCOMs onshore were grouped into a single static shunt reactor with a rating of 250 MVA. This rating was chosen empirically to achieve stable voltage conditions at rated wind speed. Finally, the onshore grid was modeled as a 230 kV ideal source with a series impedance.

III. Proposed Export Cable Protection Scheme

This section presents the proposed OWF export cable protection scheme. Fig. 5 shows an overview of the proposed protection scheme for export cable EXP1a. Identical protection schemes were implemented for the other export cables. Two circuit breakers (CBs) were placed on EXP1a along with two multi-function relays. Current transformers (CTs) and potential transformers (PTs) were placed on the bus side of each CB to supply secondary currents and voltages to the relays. Differential relays were placed both offshore and onshore. However, distance protection was only provided onshore, because the only generation sources offshore were the WTGs, which are known to inject unconventional fault current. The presence of the grid onshore provided a stronger and more conventional fault current to be used by the distance relay. In case of a fault, contribution was provided from three sources: the aggregated WTG, the onshore grid, and the rest of the OWF.

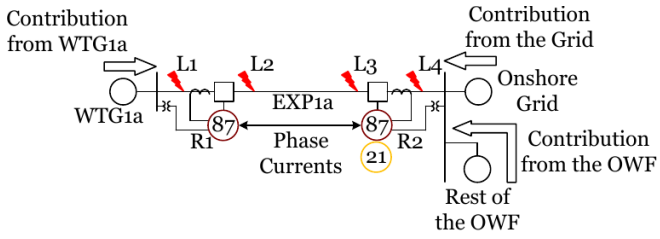

Fig. 5. Proposed export cable protection scheme overview.

A. Overview of the Current Differential Scheme

This section covers the proposed primary protection scheme for in-zone faults. Fig. 6 shows the logic for a line current differential scheme used as the primary protection of EXP1a.

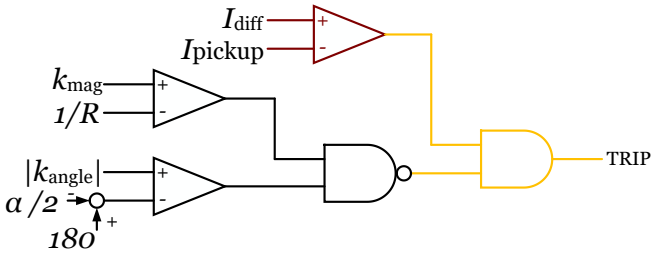

Fig. 6. Differential scheme logic.

For this logic to issue a differential trip in response to the measured quantities, the output of both the alpha plane comparator and the overcurrent comparator had to be high. Fig. 7 shows the alpha plane, where the boundaries of the operate and restrain regions were dictated by R and α. The relay calculated the ratio of the local current phasor I_{local} to the remote current phasor I_{remote}, resulting in the calculation of a complex ratio k using (8):

$$k = \frac{I_{local}}{I_{remote}}. \quad (8)$$

k was then plotted to determine whether it lay within the restrain or operate region. If k was within the operate region, the first condition of the differential logic was met. For the second condition, the differential current magnitude was compared to a pickup setting to ensure that enough current was present to declare a fault. For this study, only phase- and zero-sequence differential functions were employed, because WTGs do not generate negative-sequence current. The identical phase was set at $R = 6$, and the zero-sequence alpha plane was set at $\alpha = 195$, which are the manufacturer's recommended default values. The overcurrent pickup for phase current quantities was set at 1.2 pu, and the pickup for zero-sequence currents was set at 0.1 pu, which are also the manufacturer-recommended default values. These set points were identical for both offshore and onshore relays. The rationale for using these settings was to be able to compare the overcurrent logic scheme to more common differential applications that perform reliably using default set points.

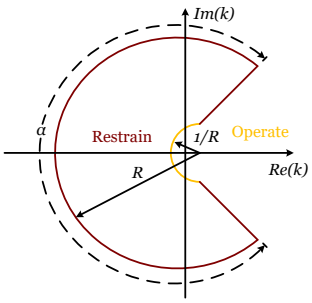

Fig. 7. Differential protection alpha plane.

B. Overview of the Distance Scheme

Additional protection functions are often enabled to provide backup coverage for the primary scheme. In this study, a distance protection scheme was enabled at the onshore relay station to back up the differential relay for line-to-line faults. Distance protection schemes calculated a measured impedance using local voltage and current signals. Then the impedance was plotted on the complex plane to determine if it lay within any of the predefined operating zones. Fig. 8 depicts the impedance characteristics used to determine if a fault condition were present. Two overlapping regions in Fig. 8 were designated as Zone 1 and Zone 2.

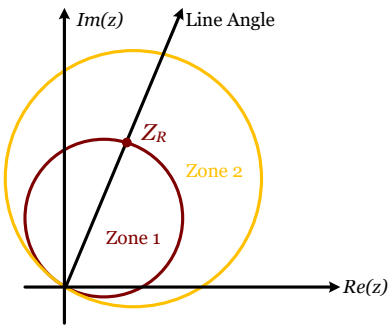

Fig. 8. Distance protection impedance plane.

Settings for the impedance zones were determined using the export cable impedance. Zone 1 was set to detect faults between 0-80% impedance, while Zone 2 was to detect fault at up to 150% impedance. Since Zone 1 did not overreach the remote terminal at the offshore substation, it was set to operate with no intentional time delay. Zone 2 was set to operate with a 42-cycle delay to allow the primary protection at the offshore platform the chance to clear the fault first.

In the selected relays, a distance scheme trip could not be issued unless the relay declared the fault to be in the forward direction. Directionality in relays is determined using sequence quantities derived from phase voltages and currents. For phase faults, the relay uses negative-sequence and phase-voltage polarized elements to declare a directional decision; however, the relay gives priority to the negative-sequence calculation. Directional settings in the onshore relay were set using the manufacturer- recommended guidelines to compare its performance with more conventional protection schemes.

TABLE I
PERFORMANCE SUMMARY FOR OFFSHORE RELAY R1

Fault Location	Operating Element			Operating Time		
	ABCG	AB	AG	ABCG	AB	AG
L1 (Reverse)	––	––	––	––	––	––
L2 (In-Zone)	87OP	87OP	87OP	4 ms	16.667 ms	8 ms
L3 (In-Zone)	87OP	87OP	87OP	8 ms	12.5 ms	8 ms
L4 (Out-of-Zone)	––	––	––	––	––	––

TABLE II
PERFORMANCE SUMMARY FOR ONSHORE RELAY R2

Fault Location	Operating Element			Directionality Results			Operating Time		
	ABCG	AB	AG	ABCG	AB	AG	ABCG	AB	AG
L1 (Out-of-Zone)	Z2P Distance	Z2P Distance	51G	F32P	F32P	F32V	708.47 ms	704.16 ms	855 ms
L2 (In-Zone)	87OP	87OP	87OP	F32P	F32P	F32V	4 ms	16.667 ms	8 ms
L3 (In-Zone)	87OP	87OP	87OP	F32P	F32P	F32V	8 ms	12.5 ms	8 ms
L4 (Reverse)	Z1P Distance	Z1P Distance	––	F32P	F32P	R32V	––	––	–

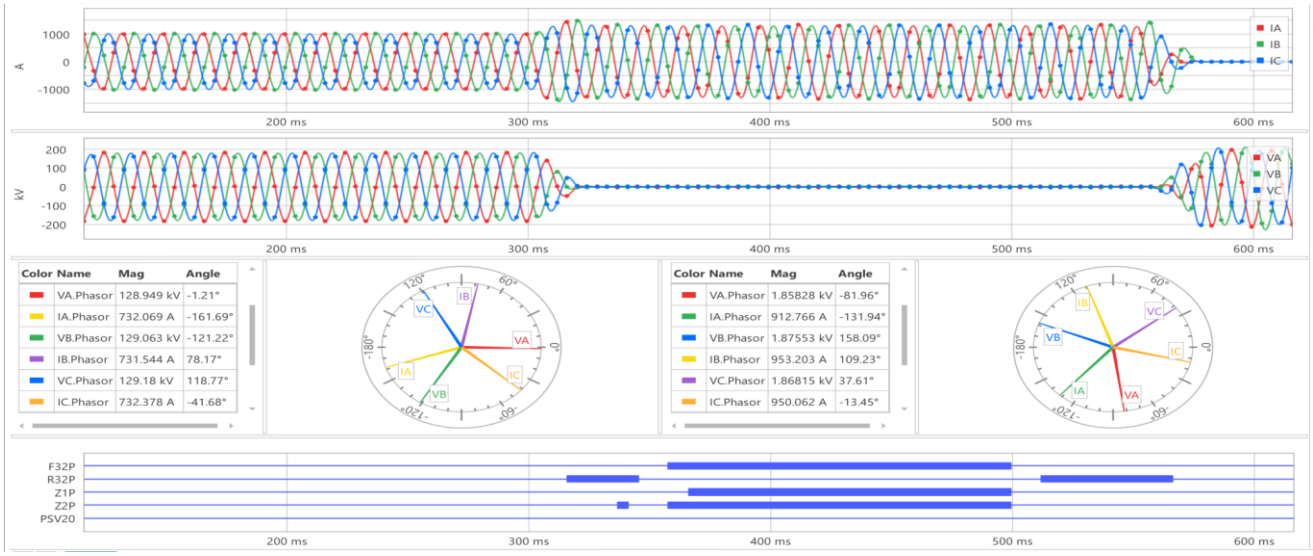

Fig. 9. Event report for relay R2 for an ABCG fault at L4.

IV. PERFORMANCE EVALUATION

A. Initial Scheme Performance

This section describes the experiment set-up and analysis used to assess the performance of the protection scheme The experimental setup designed for HIL testing consisted of two physical relays connected to each other using optical fiber cables. The physical relays used line-current-differential relaying for primary protection and distance relaying as backup. The relays were electrically connected to one real-time digital simulator (RTDS) rack using a giga- transceiver analog output (GTAO) card. Because the output signal from the GTAO card is low-power, two power amplifiers were used to amplify the signals from RTDS to the relays. To evaluate the performance of the proposed scheme, the protection coordination setting files were first uploaded to each relay. Then, ABCG, AB, and AG faults were applied at locations L1, L2, L3. and L4 (previously shown in Fig. 5). Finally, event

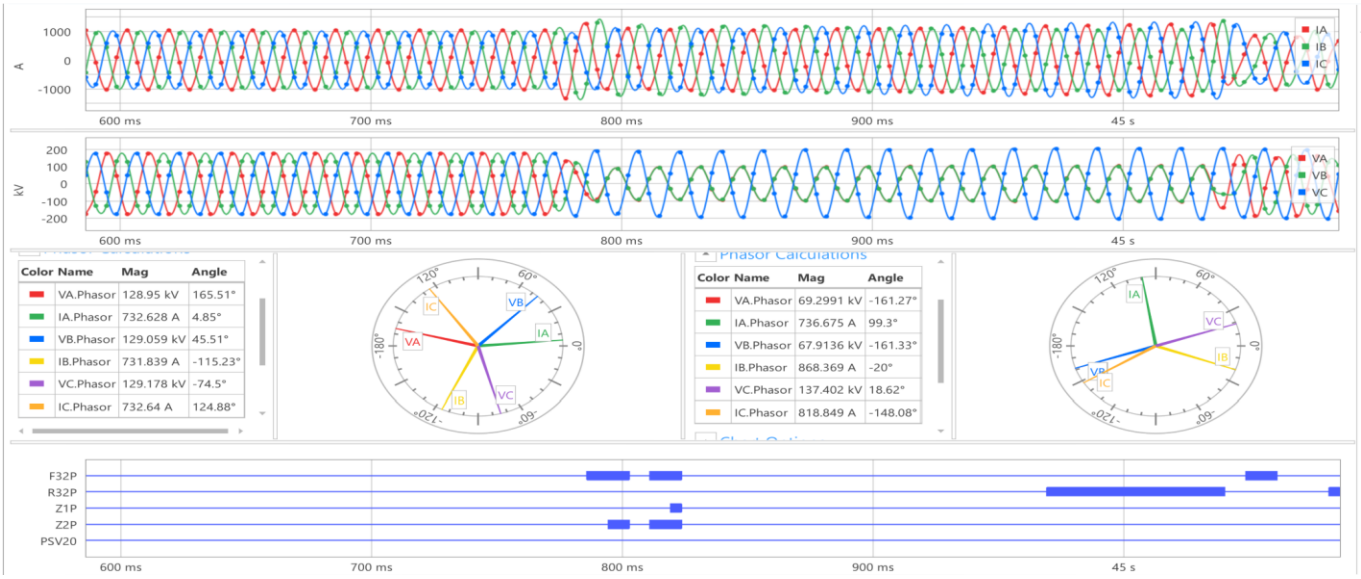

Fig. 10. Event report for relay R2 for an AB fault at L4.

report files were extracted from the relays to further analyze the performance.

Tables I and II summarize the performance of the proposed method. Both offshore and onshore differential relays operated correctly under all scenarios, within a fraction of a cycle. The onshore distance relay operated correctly for forward out-of-zone faults. However, it misoperated under reverse ABCG and AB faults onshore, because for faults at L1, the distance relay measured current from the grid, which has a more conventional fault current response. Conversely for faults at L4, the distance relay measured current from the WTG, which has an unconventional form. Fig. 9 shows the event report for relay R2 for an ABCG fault at L4. The peak magnitude of the pre-fault current was approximately 1000 A. As soon as the fault occurred, the current increased to nearly 1100 A. The relay bits initially declared a reverse direction; however, moments later a false forward direction was declared. Additionally, the relay detected the fault as being in Zone 1, which then falsely issued an instantaneous trip. Since the fault current waveform became distorted after the fault, the phase directionality and impedance calculation elements failed which, in turn, caused the distance relay to misoperate.

Fig. 10 shows the event report of relay R2 for an AB fault at L4. Initially, the relay declared a forward fault as well as an out- of-zone fault. However, moments later a Zone 1 trip was declared, and a false instantaneous trip was issued because the fault current waveform was distorted. Interestingly, all three phases exhibited roughly equal magnitudes of fault current even though the fault was only between A and B phase.

B. Proposed Loss-of-Potential Overcurrent Logic

An alternative backup protection scheme proposed by this study was designed to combat the directionality issues in the distance scheme. This alternative relied on a voltage-supervised overcurrent function to detect faults, and its logic is shown in Fig. 11. A simple overcurrent scheme is less susceptible to the distortion contained in analog voltages and currents since it only requires that the current magnitude be accurate. To add additional security to this scheme, this element was restrained when the voltage was above 75 percent of its nominal value. This mitigated any loadability issues that the overcurrent element introduced. The pickup setting was determined by taking the maximum possible load current on EXP1a and adding a safety factor of 150%. This also ensured that any measured current quantity above the pickup was only a result of fault conditions. No directional control was needed for this proposed logic, since it is impossible under reverse faults for the measured current to exceed the pickup setting. Figs. 9 and 10 show that the proposed overcurrent logic was not affected by the current waveform and the logic prevented the relay from misoperating. This is evidenced by the PSV20 bit remaining de-asserted throughout the event.

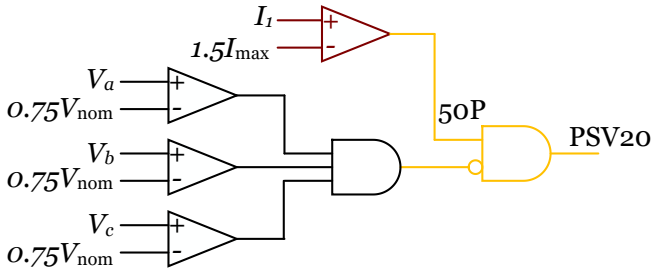

Fig. 11. Proposed loss-of-potential overcurrent logic.

V. Conclusions

This paper proposes an export cable protection system for OWFs that use Type-IV WTGs. Primary protection was provided using current differential protection by placing two relays on each export cable. Distance protection was provided

as a backup onshore in case communication was lost. However, since it is known that distance protection is likely to fail with WTGs, this paper proposed overcurrent logic as alternative backup protection. An experimental setup was created using a real-time digital simulator, physical relays, and power amplifiers. The scheme's performance was evaluated using HIL testing. The HIL results demonstrated that the proposed protection scheme operated correctly for all types of faults at all locations. The distance backup scheme operated correctly for forward out-of-zone faults, both offshore and onshore. However, it misoperated for reverse ABCG and AB faults onshore. The HIL test results showed that using the overcurrent logic protection scheme prevented the relay from misoperating and maintained successful protection coordination to ensure the safe and reliable delivery of power from the OWF.

VI. Future Work

Aspects of this alternative protection scheme can be studied in the future, starting with the STATCOM devices onshore, which have a similar fault current response to WTGs. Since these STATCOMs are large, their fault current contribution may affect the operation of the proposed protection scheme. Therefore, a detailed or black box, real-time model of the STATCOMs needs to be developed to analyze their impact on the operation of the proposed scheme. Second, since the WTGs' fault-current response is affected by their low-voltage, ride-through control unit, this unit should be added to the model to further analyze its impact on the proposed scheme. Finally, the WTG models could be further enhanced to analyze the impact of their generation on the performance of the proposed scheme.

References

[1] T. Kauffmann, U. Karaagac, I. Kocar, S. Jensen, E. Farantatos, A. Haddadi, and J. Mahseredjian, "Short-circuit model for Type-IV wind turbine generators with decoupled sequence control," *IEEE Trans. Power Del.*, vol. 34, no. 5, pp. 1998–2007, Oct. 2019.

[2] R. Chowdhury and N. Fischer, "Transmission line protection for systems with inverter-based resources – Part I: Problems," *IEEE Trans. Power Del.*, vol. 36, no. 4, pp. 2416–2425, Aug. 2021.

[3] A. Haddadi, M. Zhao, I. Kocar, U. Karaagac, K. W. Chan, and E. Farantatos, "Impact of inverter-based resources on negative sequence quantities-based protection elements," *IEEE Trans. Power Del.*, vol. 36, no. 1, pp. 289–298, Feb. 2021.

[4] H. Ghaffarzadeh and A. Mehrizi-Sani, "Review of control techniques for wind energy systems," *Energies*, vol. 13, no. 24, Dec. 2020.

[5] H. Ghaffarzdeh and A. Mehrizi-Sani, "Mitigation of subsynchronous resonance induced by a Type III wind system," *IEEE Trans. Sust. Energy*, vol. 11, no. 3, pp. 1717–1727, Jul. 2020.

[6] A. Mohammadhassani, N. Skoff, and A. Mehrizi-Sani, "Performance analysis of distance protection in presence of Type III wind turbine generators," *IEEE Power Energy Soc. Innov. Smart Grid Tech. Conf.*, pp. 1–5, Feb. 2021.

[7] A. Mohammadhassani, A. Mehrizi-Sani, and K. Saleh, "Fault current directionality in islanded microgrids using SVM and synthetic harmonic injection," *IEEE Intl. Symp. Ind. Electron.*, pp. 1–5, Jun. 2021.

[8] L. He, C.-C. Liu, A. Pitto, and D. Cirio, "Distance protection of AC grid with HVDC-connected offshore wind generators," *IEEE Trans. Power Del.*, vol. 29, no. 2, pp. 493–501, Apr. 2014.

[9] M. Zolfaghari, R. M. Chabanlo, M. Abedi, and M. Shahidehpour, "A robust distance protection approach for bulk AC power system considering the effects of HVDC interfaced offshore wind units," *IEEE Syst. J.*, vol. 12, no. 4, pp. 3786–3795, Dec. 2018.

[10] K. El-Arroudi and G. Joos, "Performance of interconnection protection´ based on distance relaying for wind power distributed generation," *IEEE Trans. Power Del.*, vol. 33, no. 2, pp. 620–629, Apr. 2018.

[11] Y. Fang, K. Jia, Z. Yang, Y. Li, and T. Bi, "Impact of inverter-interfaced renewable energy generators on distance protection and an improved scheme," *IEEE Trans. Ind. Electron.*, vol. 66, no. 9, pp. 7078–7088, Sep. 2019.

[12] R. Chowdhury and N. Fischer, "Transmission line protection for systems with inverter-based resources – Part II: Solutions," *IEEE Trans. Power Del.*, vol. 36, no. 4, pp. 2426–2433, Aug. 2021.

[13] Y. Liang, W. Li, and Z. Lu, "Effect of inverter-interfaced renewable energy power plants on negative-sequence directional relays and a solution," *IEEE Trans. Power Del.*, vol. 36, no. 2, pp. 554–565, Apr. 2021.

[14] B. Brusilowicz and N. N. Schulz, "Polarizing voltage generating method for distance and directional protection elements," *IEEE Trans. Power Del.*, vol. 36, no. 1, pp. 74–83, Feb. 2021.

[15] S. Biswas, P. K. Nayak, and G. Pradhan, "A dual-time transform assisted intelligent relaying scheme for the STATCOM-compensated transmission line connecting wind farm," *IEEE Syst. J.*, vol. 16, no. 2, pp. 2160–2171, Jun. 2022.